

Testing scalar dark matter clumps with Pulsar Timing Arrays

Philippe Brax and Patrick Valageas

Université Paris-Saclay, CNRS, CEA, Institut de physique théorique, 91191, Gif-sur-Yvette, France

Scalar dark matter is a viable alternative to particle dark matter models such as Weakly Interacting Massive Particles (WIMPs). This is particularly the case for scalars with a low mass $m \gtrsim 10^{-21}$ eV as required to make quantum effects macroscopic on galactic scales. We point out that by synchronising the measurements of arrival times of pairs of pulsars, Pulsar Timing Arrays (PTA) could probe ultralight dark matter (ULDM) scenarios with a mass 10^{-23} eV $\lesssim m \lesssim 10^{-19}$ eV that is greater than the one reached in standard analysis. The upper limit on the mass m is set by the time lag Δt between the observations of the two pulsars and could be pushed above 10^{-19} eV for Δt smaller than one hour. However, for these high scalar masses only very high density dark matter clouds could be detected and the capture rate of neutron stars is too low to provide sufficient statistics. Significant detection probabilities would thus require direct dark-matter-baryon interactions that favor the formation of neutron stars within such dark matter clouds, or the discovery of black hole/pulsar binary systems, taking advantage of the dark matter spike generated by the black hole.

I. INTRODUCTION

The range of possible masses for the dark matter particles has been largely extended in the last few years [1]. Of particular interest is the low mass region below $m \lesssim 1$ eV where dark matter behaves like a classical field whose non-relativistic limit is well approximated by a Schrödinger equation. When the mass is low enough, around $m \sim 10^{-22}$ eV, the quantum properties of the dark matter field at the de Broglie length can reach galactic sizes [2, 3]. Self-interactions alter this picture. In particular quartic self-interactions give rise to a Gross-Pitaevski equation with cubic terms in the Schrödinger equation. This can change the small distance properties of dark matter as solitons can emerge that are governed by the balance between gravity and the repulsive self-interactions. They have a well-defined size r_a related to the self-interaction coupling and the scalar mass [4–6]. As such they can be candidates for modifying the small-scale properties of dark matter halos, i.e. they render them smooth on scales lower than r_a . In addition, they can display peculiar features such as vortex lattices, similar to those found in laboratory experiments on superfluids [7, 8]. Self-interacting model can be relevant astrophysically for a larger range of masses than the free fuzzy dark matter case. Testing scalar dark matter models with larger masses is one of the aims of this article.

The solitons can also have much smaller radii than galactic sizes and represent clumps of dark matter [9, 10]. In this case, their central density can be much larger than the one averaged on a kpc scale or the upper bound found in the Earth’s environment. In particular, dense clumps could surround far away objects such as pulsars or binary black holes. In the latter case, the evolution of the binary system can be affected by the dynamical friction exerted by the dark matter environment [11, 12]. In addition, the propagation of the gravitational waves emitted by the binary system is affected by the oscillatory component of the Newtonian potential in the clump, at a pulsation of twice the scalar mass $\omega = 2m$. This could

be detected in the future by LISA or DECIGO if the clumps form around the matter-radiation equality and the dark matter mass is between 10^{-23} eV and 10^{-21} eV [13, 14]. This could also be detected in Pulsar Timing Arrays (PTA) through the impact on the propagation time of the signal from each pulsar [15]. This is equivalent to the Sachs-Wolfe effect for the Cosmic Microwave Background (CMB). Numerical simulations have shown that dark matter solitons are typically embedded within extended virialized envelopes that exhibit strong density fluctuations on the de Broglie scale [6, 16]. These fluctuations can be described as quasi-particles [3] and they could also be probed by gravitational waves interferometers and PTA [17–19]. The PTA results can have important consequences for fundamental physics [20] and in particular dark matter such as the existence of WIMPs [21] or ultra-light dark matter (ULB) [22–25]. On the other hand, if the dark matter is coupled to the neutrinos its coherent oscillation can impact the propagation of the neutrinos and be detected in oscillation experiments [26, 27].

In this paper we revisit the effect associated with the coherent oscillation of the dark matter gravitational potential inside solitons, focusing on the correlation between two signals coming from two pulsars [28]. We point out that in the presence of a dark matter clump around each pulsar, the cross-correlation exhibits a low-frequency signal, $\omega \ll m$. Moreover, high scalar masses could be probed if the observations of the two pulsars are synchronised. We evaluate the signal-to-noise ratio (SNR) when taking into account the white and red noises in the arrival times. A conservative bound on the SNR allows us to predict that a wider range of scalar masses can be tested by PTA experiments, with masses up to $m \simeq 10^{-19}$ eV for time-lags of one hour between the two pulsars. Interestingly, this signal would also be prominent when the dark matter clumps have a density close to the one at matter-radiation equality. This is in the same ballpark as the detectability of scalar clumps by LISA or DECIGO. As a result the study of such correlations in the PTA data would certainly give us clues

to what can be expected from future gravitational wave experiments. The synergy between the two types of astronomical observables is worth pursuing, we intend to come back to it in the future.

The paper is arranged as follows. In a first part **II** we recall the essential ingredients of ultra light dark matter and the corresponding Sachs-Wolfe effect in dark matter clumps. In section **III**, we introduce the correlation between the arrival times and consider the SNR for the filtered signal at low frequency. In section **IV**, we derive quantitative results and compare this approach with standard pulsar time delay analysis. In App. **A** we derive the contribution of the red noise to the variance of the signal. In App. **B** we estimate the encounter and capture probabilities of a neutron star by a scalar dark matter cloud.

II. ULTRALIGHT DARK MATTER

A. Oscillating scalar field

We consider ultra-light dark matter scenarios, where a scalar field $\phi(\vec{x}, t)$ is governed by the Lagrangian density

$$\mathcal{L}_\phi = -\frac{1}{2}(\partial\phi)^2 - \frac{m^2}{2}\phi^2 - \frac{\lambda_4}{4}\phi^4, \quad (1)$$

where λ_4 is the self-interaction coupling constant. These self-interacting scalars could play a role at short distance on sub-galactic scales and make solitons which could alleviate some of the small-scale dark matter conundra. In the Newtonian gauge $ds^2 = -(1 + 2\Phi)dt^2 + (1 - 2\Psi)d\vec{x}^2$ and in the weak-gravity regime, the scalar field obeys, at leading order, the Klein-Gordon equation

$$\ddot{\phi} - \vec{\nabla}^2\phi + (1 + 2\Phi)m^2\phi + \lambda_4\phi^3 = 0. \quad (2)$$

Here we assumed that the self-interactions are small, $\lambda_4\phi^4 \ll m^2\phi^2$, so that at zeroth order the scalar field oscillates in the harmonic potential $m^2\phi^2/2$, with a vanishing pressure P and a constant density ρ . Here $\Phi = \Psi$ is the constant Newtonian potential at leading order. As pointed out by [15], we shall recall below in Eqs.(12)-(15) that there are also subleading oscillating components in the density, pressure and gravitational potential, as well as a small mean pressure, which is subdominant in the nonrelativistic regime.

In the nonrelativistic regime, it is convenient to introduce a complex scalar field ψ with [3]

$$\phi = \frac{1}{\sqrt{2m}} (e^{-imt}\psi + e^{imt}\psi^*), \quad (3)$$

which obeys the Schrödinger equation

$$i\dot{\psi} = -\frac{\vec{\nabla}^2\psi}{2m} + m(\Phi + \Phi_I)\psi, \quad \Phi_I = \frac{3\lambda_4}{4m^3}|\psi|^2. \quad (4)$$

This can be mapped to an hydrodynamical picture through the Madelung transform [29]

$$\psi = \sqrt{\frac{\rho}{m}} e^{iS}, \quad \vec{v} = \frac{\vec{\nabla}S}{m}, \quad (5)$$

which leads to the continuity and Hamilton-Jacobi equations

$$\dot{\rho} + \frac{\vec{\nabla} \cdot (\rho \vec{\nabla}S)}{m} = 0, \quad (6)$$

$$\dot{S} + \frac{(\vec{\nabla}S)^2}{2m} = -m(\Phi_Q + \Phi + \Phi_I), \quad \Phi_Q = -\frac{\vec{\nabla}^2\sqrt{\rho}}{2m^2\sqrt{\rho}}, \quad (7)$$

where we introduced the quantum pressure Φ_Q . Taking the gradient of Eq.(7) gives the Euler equation, with an effective pressure due to the quantum pressure Φ_Q and the self-interaction potential Φ_I .

These equations of motion typically lead to the formation of hydrostatic equilibria, also called solitons or bosons stars, which may be embedded within a larger virialized halo governed by velocity dispersion [6]. Whereas the soliton is a ground state associated with a vanishing velocity dispersion and a smooth density profile over a large radius R_0 , the outer envelope displays large density fluctuations over the de Broglie wavelength λ_{dB} . Typically we consider the regime where the soliton has a size larger than the de Broglie wavelength and is the result of the equilibrium between the scalar pressure (repulsive) and gravitation.

In this paper, we consider the case where pulsars could be located within dark matter solitons. Denoting by \vec{v}_0 the collective velocity of the soliton, the hydrostatic equilibrium that determines the density profile of the soliton reads $\Phi_Q + \Phi + \Phi_I = \text{constant}$, and as seen from Eq.(7) the phase reads

$$S = -\mu mt + m\vec{v}_0 \cdot \vec{x} - \alpha, \quad \mu = \frac{v_0^2}{2} + \Phi_Q + \Phi + \Phi_I, \quad (8)$$

where α is a constant phase offset. Going back to the scalar field ϕ , this gives

$$\phi = \frac{\sqrt{2\rho}}{m} \cos(Et + \beta), \quad \beta = \alpha - m\vec{v}_0 \cdot \vec{x}, \quad (9)$$

and

$$E = m(1 + \mu) = m \left(1 + \frac{v_0^2}{2} + \Phi_Q + \Phi + \Phi_I \right). \quad (10)$$

We can check that this is a solution of the Klein-Gordon equation (2) in the nonrelativistic regime, $|\mu| \ll 1$, after averaging over the fast oscillations.

B. Oscillating gravitational potentials

The oscillating scalar field (9) actually leads to both constant and oscillating components in the scalar-field

energy-momentum tensor T_ν^μ [15],

$$-T_0^0 = \bar{\rho} + \rho_{\text{osc}}, \quad T_i^i = 3(\bar{P} + P_{\text{osc}}), \quad (11)$$

with at leading order $\bar{\rho} = \rho$,

$$\rho_{\text{osc}} = -\rho \cos(2\theta) \left(v_0^2 + \bar{\Phi}_Q + \frac{1}{3}\bar{\Phi}_I \right) + \rho \cos(4\theta) \frac{1}{6}\bar{\Phi}_I, \quad (12)$$

where we denote $\theta = Et + \beta$ the argument of the cosine in Eq.(9), and

$$\bar{P} = \rho \left(\frac{v_0^2}{3} + \bar{\Phi}_Q + \frac{\bar{\Phi}_I}{2} \right), \quad P_{\text{osc}} = -\rho \cos(2\theta). \quad (13)$$

Thus, whereas $\rho_{\text{osc}} \ll \bar{\rho}$ we have $\bar{P} \ll P_{\text{osc}}$ in the nonrelativistic regime. From the Einstein equations,

$$-2\bar{\nabla}^2 \Psi = 8\pi\mathcal{G}T_0^0, \quad 6\ddot{\Psi} - 2\bar{\nabla}^2(\Psi - \Phi) = 8\pi\mathcal{G}T_i^i, \quad (14)$$

we obtain for the gravitational potential Ψ

$$\nabla^2 \bar{\Psi} = 4\pi\mathcal{G}\rho_0, \quad \Psi_{\text{osc}} = \frac{\pi\mathcal{G}\rho_0}{m^2} \cos(2\theta). \quad (15)$$

The second equation gives access to the oscillating part of the Newtonian potential induced by the rapid oscillations of the matter density.

C. Sachs-Wolfe effect and time delays

As for the Sachs-Wolfe effect for the Cosmic Microwave Background (CMB), when photons travel from a pulsar towards the Earth, their frequency is modified by the metric fluctuations as [15]

$$\frac{f_e - f_p}{f_p} = \int_{t_p}^{t_e} dt \partial_t (\Phi + \Psi) + \Phi_p - \Phi_e. \quad (16)$$

Here we denote with the subscript e and p the time and location associated with the Earth and the pulsar. The time-independent components $\bar{\Psi}$ and $\bar{\Phi}$ of the gravitational potentials lead to a constant frequency shift that cannot be measured, as we do not know with exact accuracy the value of the emission frequency f_p . Therefore, in the following we focus on the oscillatory components of the metric potentials. Writing $\partial_t = \frac{d}{dt} - n_i \partial_i$, where \vec{n} is the unit vector along the signal propagation, and integrating, we obtain [15]

$$\frac{f_e - f_p}{f_p} = \Psi_e - \Psi_p - \int_{t_p}^{t_e} dt n_i \partial_i (\Phi + \Psi). \quad (17)$$

The integrated effect is suppressed by a factor k/m where k is the wave number. Assuming that the gravitational potential is much deeper in the dark matter cloud around the pulsar than around the Earth, we approximate the frequency shift by

$$\frac{\delta f}{f}(t) = -\Psi_p \cos(2E_p(t - d_p) + 2\beta_p), \quad (18)$$

where we wrote $t_p = t_e - d_p$, with d_p the distance to the pulsar, and $\Psi_p = \pi\mathcal{G}\rho_p/m^2$ from Eq.(15), where ρ_p is the density of the dark matter soliton around the pulsar. As explained above, here we focus on the time-dependent frequency shift.

The frequency shift leads to a time delay δt of the pulses measured on the Earth,

$$\delta t = - \int_0^t dt \frac{\delta f}{f}. \quad (19)$$

Keeping again only the time-dependent component, this gives

$$\delta t = \frac{\Psi_p}{2m} \sin(2E_p t + \gamma_p), \quad \gamma_p = -2E_p d_p + 2\beta_p. \quad (20)$$

In standard analysis of pulsar timing array data [15, 22, 30, 31], one directly uses Eq.(20) to search for an ultralight dark matter signal in the set of times of arrival. In this approach, one approximates $E_p \simeq m$, so that all pulsars may lead to an oscillatory signal with the same frequency $f = m/\pi$. If the dark matter cloud is very large ($m \lesssim 10^{-22}$ eV) and contains the Earth as well as all the pulsars, one includes the Earth term and all terms have the same amplitude. This leads to constraints on ultralight dark matter scenarios with $m \lesssim 10^{-22}$ eV. This upper limit is set by the typical time interval ΔT_{obs} between two measurements, which sets an upper bound on the frequency $f_{\text{max}} = 1/\Delta T_{\text{obs}}$ that can be measured from the data. With $\Delta T_{\text{obs}} \simeq 1$ week, this gives $f_{\text{max}} \sim 2 \times 10^{-6}$ Hz and $m_{\text{max}} = \pi f_{\text{max}} = 3 \times 10^{-21}$ eV. A more careful analysis shows that these data provide constraints in the range 10^{-24} eV $\lesssim m \lesssim 10^{-22}$ eV, as one needs at least a few points in a cycle to extract the signal [31].

III. MOVING THE OBSERVATIONAL WINDOW TO HIGHER SCALAR MASS

A. Correlation of a pair of pulsars

In this paper, we investigate whether one can constrain higher dark matter masses m by cross-correlating the signals from different pulsars. Indeed, considering two pulsars a and b measured at times t_{ai} and t_{bj} , we obtain

$$\delta t_{ai} \delta t_{bj} = \frac{\Psi_a \Psi_b}{4m^2} \sin(2E_a t_{ai} + \gamma_a) \sin(2E_b t_{bj} + \gamma_b). \quad (21)$$

This also reads

$$\delta t_{ai} \delta t_{bj} = \frac{\Psi_a \Psi_b}{8m^2} \left[\cos(2E_a t_{ai} - 2E_b t_{bj} + \gamma_a - \gamma_b) - \cos(2E_a t_{ai} + 2E_b t_{bj} + \gamma_a + \gamma_b) \right]. \quad (22)$$

If $t_{ai} = t_{bj} = t$, the second term oscillates at the angular frequency $\omega \simeq 4m$, which is the second harmonic of the one-point signal (20), and does not give access to

higher scalar mass m . However, the first term oscillates at the much smaller angular frequency $\omega = 2(E_a - E_b) = 2m(\mu_a - \mu_b) \ll 2m$. For a fixed range of frequency probed by an experiment, this could provide constraints on much higher scalar masses m . Moreover, by filtering the signal as in Eq.(26) below, one can reach high scalar masses up to $m \lesssim 1/|\Delta t_{ij}|$ as in Eq.(27) below, where Δt_{ij} is the time-lag between the measurements of the two pulsars. This upper mass limit could thus be pushed to high values. The goal of this paper is to investigate these points.

Defining the means and differences

$$\bar{\mu} = \frac{\mu_a + \mu_b}{2}, \quad \Delta\mu = \frac{\mu_a - \mu_b}{2}, \quad \bar{\gamma} = \frac{\gamma_a + \gamma_b}{2}, \quad \Delta\gamma = \frac{\gamma_a - \gamma_b}{2}, \quad (23)$$

and

$$\bar{t}_{ij} = \frac{t_{ai} + t_{bj}}{2}, \quad \Delta t_{ij} = \frac{t_{ai} - t_{bj}}{2}, \quad (24)$$

the product (22) reads

$$\delta t_{ai} \delta t_{bj} = \frac{\Psi_a \Psi_b}{8m^2} [\cos(4m(1+\bar{\mu})\Delta t_{ij} + 4m\Delta\mu\bar{t}_{ij} + 2\Delta\gamma) - \cos(4m(1+\bar{\mu})\bar{t}_{ij} + 4m\Delta\mu\Delta t_{ij} + 2\bar{\gamma})]. \quad (25)$$

We shall sum over measurements with small time intervals Δt_{ij} (i.e., the two pulsars are observed at two closely separated times) while \bar{t}_{ij} can span a few years (the duration T_{obs} of the observational campaign). The second term oscillates with \bar{t}_{ij} at the fast angular frequency $4m(1+\bar{\mu})$ whereas the first term oscillates more slowly at the angular frequency $4m\Delta\mu$. To distinguish this small oscillatory component in the data, we multiply the time delays by a similar oscillatory filter and we define the observable

$$s = \frac{1}{N_{ij}} \sum_{ij} \delta t_{ai} \delta t_{bj} \cos(4\omega\bar{t}_{ij}), \quad (26)$$

where we sum over a set of N_{ij} pairs of times of arrival $\{t_{ai}, t_{bj}\}$ and $\omega > 0$. In the regime

$$4mT_{\text{obs}} \gg \pi, \quad 4m|\Delta t_{ij}| \ll \pi, \quad |m|\Delta\mu - \omega| T_{\text{obs}} \ll \frac{\pi}{8}, \quad (27)$$

the second term in (25) shows many oscillations that cancel out while the first term gives a dominant contribution of the form

$$s_{\text{DM}} = \frac{\Psi_a \Psi_b}{16m^2} \cos(2\Delta\gamma), \quad (28)$$

associated with a dark matter cloud around each pulsar.

B. Dark matter mass window

The regime associated with the conditions (27) corresponds to the mass window

$$\begin{aligned} m &\gg \left(\frac{T_{\text{obs}}}{1 \text{ yr}}\right)^{-1} 2 \times 10^{-23} \text{ eV}, \\ m &\ll \left(\frac{|\Delta t|}{1 \text{ hour}}\right)^{-1} 10^{-19} \text{ eV}, \\ |m|\Delta\mu - \omega &\ll \left(\frac{T_{\text{obs}}}{1 \text{ yr}}\right)^{-1} 8 \times 10^{-24} \text{ eV}. \end{aligned} \quad (29)$$

We can see that for $|\mu| \lesssim 10^{-3}$ the width over m of a probe at frequency ω is not too narrow, which makes such an analysis possible. Depending on the total observational time T_{obs} and the time difference Δt between the measurement times of two pulsars, one may probe in this fashion dark matter scenarios with masses in the range $10^{-23} \text{ eV} < m < 10^{-19} \text{ eV}$. Of course this assumes that the cadence of pulsar observations could be as high as one per hour. This has to be adapted to future forecast for such observations. Thus, our filtering method could give access to scalar masses somewhat above the standard approach, which typically probes $m \lesssim 10^{-22} \text{ eV}$. In particular, the upper bound on the scalar mass m that can be reached is set by the time lag Δt between the measurements of the two pulsars. The main point of this paper is thus that by making this time very small, for instance by observing the two pulsars on an overlapping time interval, one could have access to high m . On the other hand, to be detectable large m models would require high-density dark matter clouds, because of the $1/m^2$ factors in Eqs.(15) and (28).

The Compton wavelength reads

$$\lambda_C = \frac{2\pi}{m} = \left(\frac{m}{10^{-20} \text{ eV}}\right)^{-1} 4 \times 10^{-3} \text{ pc}. \quad (30)$$

Therefore, the dark matter clouds that could be probed by such analysis would typically have sizes above 0.01 pc, as $R > \lambda_C$. As a result, we do not consider highly dense clumps with large Newtonian potentials.

C. Noise contributions

1. Noise contributions to the timing residuals

As in standard analysis of pulsar times of arrival [31], we write the timing residuals (with respect to a specific model of the pulsar and of the motion of the Earth) as

$$\delta\mathbf{t} = \mathbf{M} \cdot \boldsymbol{\epsilon} + \mathbf{w} + \mathbf{r} + \delta\mathbf{t}_{\text{GW}} + \delta\mathbf{t}_{\text{DM}}, \quad (31)$$

where $\delta\mathbf{t}$ is the vector of the timing residuals, $\{\delta t_{ai}, \delta t_{bj}\}$. The first term on the right-hand side arises from the error $\boldsymbol{\epsilon}$ on the parameters of the underlying deterministic timing model, using a linear approximation appropriate for

small perturbations. In the following we assume that the model parameters ϵ have already been calibrated from a standard analysis of the pulsar data and we discard this term. The second term is a white noise that is left after subtracting known systematics. The third term, often denoted $\mathbf{F} \cdot \mathbf{a}$, is a red noise component. The fourth term corresponds to the stochastic gravitational wave background. The fifth term is the time delay due to the dark matter cloud, given by Eq.(20) in our case.

We assume that the noises associated with different pulsars are uncorrelated and we write

$$\langle w_{ai}w_{bj} \rangle = \delta_{ab}\delta_{ij}\sigma_{ai}^2, \quad \langle r_{ai}r_{bj} \rangle = \delta_{ab}C_a^r(t_i - t_j), \quad (32)$$

where $\langle \dots \rangle$ is the average over the noise, which we assume to be Gaussian with zero mean, and C_a^r is the correlation function of the red noise for pulsar a .

We also write the stochastic gravitational wave background as a Gaussian noise of zero mean, with a pulsar correlation Γ_{ab} given by the Hellings & Downs overlap reduction function [32],

$$\langle \delta t_{\text{GW}ai} \delta t_{\text{GW}bj} \rangle = \Gamma_{ab} C_{\text{GW}}(t_{ai} - t_{bj}). \quad (33)$$

We define the power spectra of the red noise and of the stochastic gravitational wave background as

$$C_a^r(t) = \int_{f_{\min}}^{f_{\max}} df \cos(2\pi ft) P_a(f), \quad (34)$$

and

$$C_{\text{GW}}(t) = \int_{f_{\min}}^{f_{\max}} df \cos(2\pi ft) P_{\text{GW}}(f), \quad (35)$$

assuming most of their contribution comes from a finite range of frequencies.

2. Statistics of measurement times

Hereafter, we assume the following observational strategy. For each measurement at time t_{ai} of the pulsar a we associate a single measurement time t_{bj} for the pulsar b (the closest available time). Thus, the observable (26) reads as a single sum over N measurement time pairs,

$$s = \frac{1}{N} \sum_{i=1}^N \delta t_{ai} \delta t_{bi} \cos(4\omega T_i), \quad T_i = \frac{t_{ai} + t_{bi}}{2}. \quad (36)$$

We assume that the measurement times are roughly equally spaced over the total observational time T_{obs} ,

$$t_{ai} = i\Delta T + \Delta t_{ai}, \quad t_{bi} = i\Delta T + \Delta t_{bi}, \quad \Delta T = \frac{T_{\text{obs}}}{N}, \quad (37)$$

where Δt_{ai} and Δt_{bi} are independent Gaussian variables of variance $\sigma_t \ll \Delta T$. We denote with the angular brackets the average over the noise, as in Eq.(32), and with an overbar the average over the measurement times Δt_{ai}

and Δt_{bi} , as in Eq.(38) below. This statistical analysis allows us to estimate the typical signal-to-noise ratio as a function of the main properties of the measurement campaign: the total observational time T_{obs} , the rough periodicity ΔT of the measurements, and the irregularity σ_t of the observations due to various technical constraints.

3. Mean signal

As the noise terms of the two pulsars are uncorrelated, as in (32), the average of the observable s over the noise is given by the contributions from the dark matter oscillations and from the stochastic gravitational wave background,

$$\overline{\langle s \rangle} = s_{\text{DM}} + s_{\text{GW}}. \quad (38)$$

The dark matter contribution (28) reads

$$s_{\text{DM}} = \frac{\Psi_a \Psi_b}{16m^2} \cos(2\Delta\gamma) = \frac{\pi^2 \mathcal{G}^2 \rho_a \rho_b}{16m^6} \cos(2\Delta\gamma), \quad (39)$$

which depends crucially on the matter density in the clumps.

The stochastic gravitational wave background contribution reads

$$s_{\text{GW}} = \Gamma_{ab} \cos[2\omega(N+1)\Delta T] e^{-2\sigma^2\omega^2} \frac{\sin(2\omega T_{\text{obs}})}{N \sin(2\omega\Delta T)} \times \int_{f_{\min}}^{f_{\max}} df P_{\text{GW}}(f) e^{-2\pi^2\sigma^2 f^2}, \quad (40)$$

where we introduced $\sigma^2 = 2\sigma_t^2$. This contribution is suppressed by the trigonometric factors for $\omega T_{\text{obs}} \gg \pi$. In the following, we assume that this contribution can be distinguished from the dark matter signal (39) thanks to its specific angular correlation Γ_{ab} and its dependence on ω .

4. Variance of the signal

a. White noise The contribution of the white noise to the variance of the observable s reads

$$\langle s^2 \rangle_w = \frac{1}{N^2} \sum_i \cos^2(4\omega T_i) \sigma_{ai}^2 \sigma_{bi}^2. \quad (41)$$

Taking $\sigma_{ai} = \sigma_a$ and $\sigma_{bi} = \sigma_b$ and averaging over the measurement times, we obtain for $\sigma_w^2 = \langle s^2 \rangle_w$ the two regimes

$$\begin{aligned} \omega T_{\text{obs}} \ll \pi : \quad \sigma_w^2 &= \frac{\sigma_a^2 \sigma_b^2}{N}, \\ \omega T_{\text{obs}} \gg \pi : \quad \sigma_w^2 &= \frac{\sigma_a^2 \sigma_b^2}{2N}. \end{aligned} \quad (42)$$

They only differ by a numerical factor coming from the averaging of \cos^2 .

b. *Red noise* The contribution of the red noise reads

$$\begin{aligned} \langle s^2 \rangle_r &= \frac{1}{2N^2} \sum_{i,i'} [\cos(4\omega(T_i - T_{i'})) + \cos(4\omega(T_i + T_{i'}))] \\ &\quad \times C_a^r(t_{ai} - t_{ai'}) C_b^r(t_{bi} - t_{bi'}). \end{aligned} \quad (43)$$

Using Eq.(34), in the regime

$$\omega \ll \frac{\pi}{T_{\text{obs}}}, \quad f_{\text{max}} \ll \frac{1}{\Delta T}, \quad N \gg 1, \quad (44)$$

the variance due to the red noise becomes

$$\sigma_r^2 = \overline{\langle s^2 \rangle_r} = \frac{1}{2T_{\text{obs}}} \int_{f_{\text{min}}}^{f_{\text{max}}} df P_a(f) P_b(f), \quad (45)$$

whereas in the regime

$$\frac{\pi}{T_{\text{obs}}} \ll \omega \ll f_{\text{min}}, \quad f_{\text{max}} \ll \frac{1}{\Delta T}, \quad N \gg 1, \quad (46)$$

it reads

$$\sigma_r^2 = \frac{1}{4T_{\text{obs}}} \int_{f_{\text{min}}}^{f_{\text{max}}} df P_a(f) P_b(f). \quad (47)$$

We give in App. A more details on the derivation of Eqs.(45) and (47).

c. *Stochastic gravitational wave background* The computation of the variance due to the stochastic gravitational wave background is similar to that of the red noise. Using $\Gamma_{aa} = 1$, in the regime (44) we obtain

$$\sigma_{\text{GW}}^2 = \frac{1 + \Gamma_{ab}^2}{2T_{\text{obs}}} \int_{f_{\text{min}}}^{f_{\text{max}}} df P_{\text{GW}}(f)^2, \quad (48)$$

while in the regime (46) we obtain

$$\sigma_{\text{GW}}^2 = \frac{1 + \Gamma_{ab}^2}{4T_{\text{obs}}} \int_{f_{\text{min}}}^{f_{\text{max}}} df P_{\text{GW}}(f)^2. \quad (49)$$

IV. NUMERICAL RESULTS

A. Signal-to-noise ratio

We define the signal-to-noise ratio SNR as

$$\text{SNR} = \left| \frac{\langle s \rangle}{\sigma_s} \right|, \quad (50)$$

where σ_s is the variance due to the white and red noises, which we add in quadrature,

$$\sigma_s^2 = \sigma_w^2 + \sigma_r^2 + \sigma_{\text{GW}}^2. \quad (51)$$

From Eqs.(42), (47) and (49), pulsar timing arrays can currently reach $\sqrt{\sigma_s} \sim 10^{-7}$ s [34]. The gravitational wave background leads to a floor for the variance σ_s^2 that can only be reduced by increasing the total observational

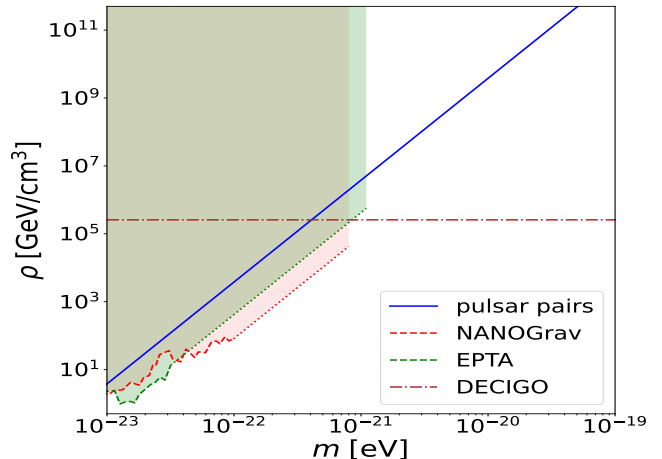


FIG. 1. The shaded regions are the exclusion domains obtained from standard pulsar time delays analysis [31, 33]. The blue solid line is our estimate (53). The horizontal dot-dashed line is the detection limit of a dark matter cloud, which would contain a white-dwarf binary system, for the observation of the waveform by the future satellite DECIGO.

time T_{obs} or by a thorough analysis of the signal taking into account its detailed spatial and temporal characteristics, in order to discriminate the dark matter signal and remove degeneracies. This goes beyond the signal-to-noise ratio estimate that we consider in this paper and is left for future work. A signal-to-noise ratio above unity corresponds to

$$\text{SNR} > 1 : \frac{\sqrt{\rho_a \rho_b}}{m^3} > \frac{4\sqrt{\sigma_s}}{\pi \mathcal{G} \sqrt{|\cos(2\Delta\gamma)|}}. \quad (52)$$

Taking for simplicity $\rho_a = \rho_b = \rho$ and $|\cos(2\Delta\gamma)| = 1/2$, this gives the detection criterion

$$\rho_{\text{SNR}} > \frac{\sqrt{\sigma_s}}{10^{-7} \text{ s}} \left(\frac{m}{10^{-20} \text{ eV}} \right)^3 5 \times 10^9 \text{ GeV/cm}^3, \quad (53)$$

which also reads

$$\rho_{\text{SNR}} > \frac{\sqrt{\sigma_s}}{10^{-7} \text{ s}} \left(\frac{m}{10^{-20} \text{ eV}} \right)^3 3 \times 10^{15} \bar{\rho}_0, \quad (54)$$

where $\bar{\rho}_0$ is the mean cosmological matter density today.

We show in Fig. 1 our result (53), which we compare with the bounds on ultralight dark matter densities already obtained by standard pulsar time delay analysis [31, 33]. We extend the bounds published in these papers to higher masses, up to $m = \pi/\Delta t$ with $\Delta t = 1$ month for [31] and $\Delta t = 3$ weeks for [33], with a slope $\rho \propto m^3$ which should hold for $m \gtrsim 1/T_{\text{obs}}$ [31]. We also display the bounds on the dark matter environment that could be obtained from the observation of gravitational waves emitted by a white-dwarf binary system by DECIGO [35, 36] following from the impact of the

dynamical friction within the dark matter cloud on the waveform [13, 37]. We can see that our method, based on the correlation of a pair of pulsars, is less efficient than the standard PTA analysis by about one to two orders of magnitude. This could be expected, as our bound corresponds to only one pair of pulsars and the analysis (53) is not necessarily optimal. A refined data analysis, with Markov-chain Monte Carlo samplers and several pulsar pairs, may somewhat improve our bound. The advantage of our approach is rather to enlarge the parameter space to higher scalar mass m . On the other hand, we can see that at these larger masses, $m \gtrsim 10^{-21}$ eV, other probes may be more competitive, such as the gravitational waves emitted by binary systems (through the impact of dynamical friction on the waveform).

We can also see that for $m \gtrsim 10^{-21}$ eV, where our new method could go beyond standard analysis, only very dense clouds could be detected, as also shown in Eq.(53). The densities found in Fig. 1 can be compared with the mean dark matter density around the solar system in the Milky Way, $\bar{\rho}_{\text{MW}} = 0.4 \text{ GeV/cm}^3$. They correspond to dark matter clouds that would be denser by a factor 10^6 at least, associated with a highly inhomogeneous dark matter density field.

B. Self-consistency checks

As seen in Eq.(15), the amplitude of the oscillating gravitational potential Ψ_{osc} is related to the density by $|\Psi_{\text{osc}}| = \pi \mathcal{G} \rho / m^2$, which reads

$$\begin{aligned} \rho_{\Psi_{\text{osc}}} &= \frac{|\Psi_{\text{osc}}|}{0.1} \left(\frac{m}{10^{-20} \text{ eV}} \right)^2 6 \times 10^{19} \text{ GeV/cm}^3 \\ &= \frac{|\Psi_{\text{osc}}|}{0.1} \left(\frac{m}{10^{-20} \text{ eV}} \right)^2 4 \times 10^{25} \bar{\rho}_0. \end{aligned} \quad (55)$$

The static gravitational potential is related to the density by $\bar{\Psi} \sim \mathcal{G} \rho R^2$, where R is the radius of the dark matter cloud. The latter must be larger than the Compton wavelength, $\lambda_C = 2\pi/m$. This gives the upper bound

$$\begin{aligned} \rho_{\bar{\Psi}} &< \frac{|\bar{\Psi}|}{0.1} \left(\frac{m}{10^{-20} \text{ eV}} \right)^2 5 \times 10^{18} \text{ GeV/cm}^3, \\ \rho_{\bar{\Psi}} &< \frac{|\bar{\Psi}|}{0.1} \left(\frac{m}{10^{-20} \text{ eV}} \right)^2 3 \times 10^{24} \bar{\rho}_0, \end{aligned} \quad (56)$$

which is somewhat stronger than (55). The fact that the signal-to-noise criterion (54) is much below the upper bounds (55) and (56) shows that the high densities required for a detection are not excluded by self-consistency arguments.

C. Representative example

Taking as a representative case at the detection limit (53),

$$m = 10^{-20} \text{ eV}, \quad \rho = 5 \times 10^9 \text{ GeV/cm}^3, \quad (57)$$

and choosing a radius $R = 0.1 \text{ pc}$, we obtain

$$R = 0.1 \text{ pc}, \quad \bar{\Psi} = 6 \times 10^{-8}, \quad \Psi_{\text{osc}} = 8 \times 10^{-12}, \quad (58)$$

while the mass of the dark matter soliton is

$$M = 5.5 \times 10^5 M_{\odot}. \quad (59)$$

Dark matter clouds with such a large density, $\rho = 3 \times 10^{15} \bar{\rho}_0$, must have formed at a redshift $z \sim 10^5$, somewhat before the matter-radiation equality. Although the clumps have relatively large masses, the fact that their Newtonian potential is so low implies that their effects on strong gravitational lensing will be small.

We estimate in App. B the encounter and capture probabilities of a neutron star with dark matter clouds as in Eqs.(58)-(59). We find that the probability of encounter of a neutron star with such a cloud, over one Hubble time, is rather low, $P_{\text{enc}} \simeq 0.003$ from Eq.(B11). The probability of capture, through the loss of energy during the crossing of the cloud by dynamical friction, is even lower, $P_{\text{cap}} \simeq 4 \times 10^{-8}$ from Eq.(B17). This result happens to be independent of the cloud properties (within its regime of validity) and is thus quite general.

Therefore, to have a chance of observing a pulsar inside such scalar dark matter clouds we would need at least 300 pulsars and a 100% capture efficiency, relying for instance on direct dark-matter-baryons interactions. A second and more promising scenario may be to increase the star formation rate inside such dark matter clouds. Then, a larger fraction of pulsars could be embedded within such clouds, simply because they were born inside rather than being captured later along their orbit in the Milky Way. Finally, a third case would be the observation of black hole/pulsar binary systems [38]. The black hole could generate a dark matter spike with a large density [39] (with a value that typically depends on the sign and amplitude of the dark matter self-interactions), which could be detected if the pulsar orbit is close enough to the black hole.

With $m|\Delta\mu| \sim m|\bar{\Psi}| \sim 10^{-26} \text{ eV}$, we can see that the third condition in (29) is simply an upper bound on ω . Here we have taken $\Delta\mu = 10^{-6}$, as from Eq.(8) we typically have $\mu \sim \max(|\Phi|, v_0^2)$, and in the case (58) we have $\Phi = \bar{\Psi} \sim 10^{-7}$ whereas we expect the clump velocities to be of the order of the typical galactic halo velocity $v_0 \sim 10^{-3}$. Therefore, such dark matter clouds could be probed by simply taking $\omega = 0$ in the definition (26) of the observable s . We hope to come back to optimising this new technique for the extraction of new physics from the PTA signal in the near future.

V. CONCLUSION

We have considered the effects of dense ultra-light dark matter clumps surrounding pulsars. The Pulsar Timing Array experiments can be used as probes of such dark matter scenarios. Indeed, in these models solitons can

form with a coherent oscillation of the underlying dark matter scalar field. This leads to a subleading oscillatory component for the local gravitational potential. These oscillations are directly transcribed via the Sachs-Wolfe effect to the arrival times of pulsar signals. As a result, the correlation between pulsar signals from different regions of space will show oscillations of two types, if these pulsars are embedded in such dark matter clumps. There is a fast oscillation coming from the coherent behaviour of the dark matter clouds at pulsation $\omega \simeq 4m$ and a lower frequency signal $\omega = 4m\Delta\mu$ arising from a beating mode due to the correlation between two pulsar signals. This is because the pulsation of the dark matter field is not exactly m but $E = m(1 + \mu)$ with $\mu = v^2/2 + \Phi_{\text{tot}}$ in the nonrelativistic regime. The fast component at $\omega \simeq 4m$ has already been studied in detail [15, 31]. In this paper we have pointed out that the slower component could allow PTAs to probe higher scalar masses.

Filtering this lower frequency component gives direct access to local properties of the clumps and is sensitive to the mass m of the scalars. Typically this pulsation is of the order of $4m \times \max(v^2/2, |\bar{\Phi}|)$, where $\bar{\Phi}$ is the gravitational potential of the clump and v its velocity, which we expect to be of the order of the rotational $v_0 \sim 10^{-3}$ in the Milky Way. We find that extracting this slow varying correlation could give access to masses for the scalar as high as 10^{-19} eV, if the time lag between the measurements of the two pulsars is of the order of one hour. If the measurements are synchronised, e.g. the pulsars are observed on overlapping time intervals, arbitrarily high dark matter masses can be probed. However, higher scalar masses require denser clumps to be detectable.

The associated clumps would be relatively large with sizes of a fraction of parsec and large masses. On the other hand as their Newtonian potential is small, they would appear as soft objects rather than compact ones, thus evading strong lensing constraints. As their density is typically larger than the one of matter-radiation equality, the observation of the slow frequency signal in the correlation between pulsar arrival times would give us a probe of the late radiation era. Surprisingly, the same regime of masses and densities would also be probed by the crossing of dark matter clumps by black hole or white dwarf binaries, as will be observed by LISA or DECIGO [13, 37]. As the PTA data are currently available, we intend to come back to the study of this range of masses 10^{-23} eV $\lesssim m \lesssim 10^{-19}$ eV where the PTA signal at low frequency could be a probe of such ultra light scalar dark matter scenarios.

Unfortunately, the capture rate of neutron stars by such scalar dark matter clumps is very low. The encounter probability of a neutron star with a dark matter cloud is below 1% and the capture probability, through dissipation by dynamical friction, is further reduced below 10^{-7} . Therefore, such dark matter clouds could only be detected by the method presented in this paper if the efficiency of the capture process reaches 100% (e.g., through direct dark-matter-baryon interactions) or

if (neutron) stars are preferentially born within such clouds. An alternative is to look for black hole/pulsar binary systems, where the dark matter spike generated by the accretion onto the black hole can reach high densities.

Appendix A: Red noise

In this appendix we detail the derivation of Eqs.(45) and (47).

In the regime (44) we can write Eq.(43) as

$$\langle s^2 \rangle_r = \frac{C_a(0)C_b(0)}{N} + \frac{1}{N^2} \sum_{i \neq i'} \int df df' P_a(f)P_b(f') \times \cos[2\pi f(t_{ai} - t_{ai'})] \cos[2\pi f'(t_{bi} - t_{bi'})], \quad (\text{A1})$$

where we used Eq.(34). Using

$$\int_{-\infty}^{\infty} \frac{dt}{\sqrt{2\pi\sigma}} e^{-t^2/(2\sigma^2)} \cos[a(t+b)] = e^{-a^2\sigma^2/2} \cos(ab), \quad (\text{A2})$$

we can integrate over the probability distribution of the Gaussian variables Δt_{ai} and Δt_{bi} , defined in (37),

$$\sigma_r^2 = \frac{C_a(0)C_b(0)}{N} + \frac{1}{N^2} \sum_{i \neq i'} \int df df' P_a(f)P_b(f') \times e^{-2\pi^2\sigma^2(f^2+f'^2)} \cos[2\pi f(i-i')\Delta T] \cos[2\pi f'(i-i')\Delta T], \quad (\text{A3})$$

where we again defined $\sigma^2 = 2\sigma_t^2$. Writing the product of cosines as a sum of two cosines and using

$$\sum_{i,i'=1}^N \cos[(i-i')\theta] = \left[\frac{\sin(N\theta/2)}{\sin(\theta/2)} \right]^2 \rightarrow N\pi\delta_D(\theta/2), \quad (\text{A4})$$

for $N \rightarrow \infty$ and $|\theta| < \pi$, we obtain in the regime (44), where $f\sigma \ll 1$, the expression (45).

In the regime (46), we keep the cosine terms $\cos(4\omega T)$ in Eq.(43), which we write as products of cosines and sines of $2\omega(t_{ai} - t_{ai'})$ and $2\omega(t_{bi} - t_{bi'})$. Then, using

$$\int_{-\infty}^{\infty} \frac{dt}{\sqrt{2\pi\sigma}} e^{-t^2/(2\sigma^2)} \cos[a(t+b)] \cos[a'(t+b)] = \frac{1}{2} e^{-(a+a')^2\sigma^2/2} \left[e^{2aa'\sigma^2} \cos[(a-a')b] + \cos[(a+a')b] \right], \quad (\text{A5})$$

and

$$\int_{-\infty}^{\infty} \frac{dt}{\sqrt{2\pi\sigma}} e^{-t^2/(2\sigma^2)} \sin[a(t+b)] \cos[a'(t+b)] = \frac{1}{2} e^{-(a+a')^2\sigma^2/2} \left[e^{2aa'\sigma^2} \sin[(a-a')b] + \sin[(a+a')b] \right], \quad (\text{A6})$$

we can integrate over the Gaussian variables Δt_{ai} and Δt_{bi} . Expanding again products of cosines and sines and using Eq.(A4), we obtain the expression (47) in the regime (46).

Appendix B: Capture rate

In this appendix we estimate the capture rate of a star by a scalar dark matter cloud. A rather similar analysis was presented in [40] for the capture of stars by the dark matter spike around primordial black holes. To be captured by the dark matter cloud, we consider that a star coming from a large distance with the relative velocity v_∞ and the impact parameter b must first enter the cloud and second dissipate enough energy ΔE by dynamical friction so that it moves from a free to a bound state.

1. Encounter rate

The number of encounters per unit time $d\Gamma$ of a star with dark matter clouds of relative velocity v_∞ and impact parameter b is given by

$$d\Gamma_{\text{enc}} = nv_\infty f(v_\infty) dv_\infty 2\pi b db, \quad (\text{B1})$$

where n is the number density of dark matter clouds while $f(v_\infty)$ is the distribution function of the relative velocity, normalized to unity. The local dark matter density in the Milky Way (along the stellar orbit), is

$$\bar{\rho}_{\text{MW}} = nM, \quad M = \frac{4\pi}{3}\rho R^3, \quad (\text{B2})$$

where ρ , M and R are the density, mass and radius of a dark matter cloud (we neglect their dispersion and assume a sharply peaked dark matter cloud distribution). This gives

$$d\Gamma_{\text{enc}} = \frac{3\bar{\rho}_{\text{MW}}}{2\rho R^3} v_\infty f(v_\infty) dv_\infty b db. \quad (\text{B3})$$

A first condition for the capture of a distant star is that it enters the cloud. Considering a hyperbolic orbit of impact parameter b and relative velocity v_∞ at infinity, the eccentricity ϵ is given by (see for instance [41] for the properties of Keplerian orbits)

$$\epsilon^2 = 1 + \frac{4v_\infty^4 b^2}{v_{\text{esc}}^4 R^2}, \quad \text{with } v_{\text{esc}}^2 = \frac{2GM}{R}, \quad (\text{B4})$$

where we introduced the escape velocity v_{esc} from the cloud. For dark matter clouds such as (58)-(59) we have

$$R = 0.1 \text{ pc}, \quad M = 5.5 \times 10^5 M_\odot : \quad v_{\text{esc}} = 217 \text{ km/s}. \quad (\text{B5})$$

As we shall see below, the relative velocity v_∞ will be much smaller than the escape velocity, $v_\infty \ll v_{\text{esc}}$, so that $\epsilon \simeq 1$ (i.e., the star is close to the limit between free and bound orbits). Then, $r_{\text{peri}} \simeq p/2$, where r_{peri} is the perihelion and p the semi-latus rectum [41], which gives

$$r_{\text{peri}} = R \frac{v_\infty^2 b^2}{v_{\text{esc}}^2 R^2}. \quad (\text{B6})$$

The condition that the star enters the cloud, $r_{\text{peri}} < R$, gives an upper bound on the impact parameter for a given relative velocity

$$b_{\text{max}} = R \frac{v_{\text{esc}}}{v_\infty} \gg R, \quad \epsilon_{\text{max}}^2 = 1 + \frac{4v_\infty^2}{v_{\text{esc}}^2} \simeq 1, \quad (\text{B7})$$

for $v_\infty \ll v_{\text{esc}}$. Thus, the assumption $\epsilon \simeq 1$ is self-consistent.

From Eqs.(B3) and (B7), the encounter rate with clouds of relative velocity below v , with $v < v_{\text{esc}}$, reads

$$\Gamma_{\text{enc}}(<v) = \frac{3\bar{\rho}_{\text{MW}}v_{\text{esc}}^2}{4\rho R} \int_0^v \frac{dv_\infty}{v_\infty} f(v_\infty), \quad (\text{B8})$$

where we integrated over b up to $b_{\text{max}}(v_\infty)$. If we neglect the velocity dispersion of the clumps, which are much more massive than the stars, and take an isotropic Gaussian of 1D dispersion σ for the 3D velocity distribution of the stars (around the mean orbital velocity at some radius r), the distribution $f(v_\infty)$ of the relative velocity is the Maxwellian distribution

$$f(v_\infty) = \frac{2}{\sqrt{2\pi}\sigma^3} v_\infty^2 e^{-v_\infty^2/(2\sigma^2)}. \quad (\text{B9})$$

This gives

$$\Gamma_{\text{enc}}(<v) = \frac{3\bar{\rho}_{\text{MW}}v_{\text{esc}}^2}{2\sqrt{2\pi}\sigma\rho R} \left(1 - e^{-v^2/(2\sigma^2)}\right). \quad (\text{B10})$$

This expression holds as long as $\sigma \lesssim v_{\text{esc}}$, so that the contribution from high-velocity stars that violate the assumption $v_\infty \ll v_{\text{esc}}$ used in (B7) is negligible. This is indeed the case as $\sigma \sim 100$ km/s [42–44] whereas we obtained in (B5) $v_{\text{esc}} = 217$ km/s. This condition on the velocity will be even satisfied better in the following section where we derive the upper bound (B15) on the star velocity by taking into account the energy loss condition.

From (B10) we then obtain the total total probability of encounter with a dark matter cloud, for a given neutron star, over a Hubble time $t_H = 1/H$,

$$P_{\text{enc}} = \Gamma_{\text{enc}} t_H = \frac{3\bar{\rho}_{\text{MW}}v_{\text{esc}}^2 t_H}{2\sqrt{2\pi}\sigma\rho R} \simeq 3 \times 10^{-3}, \quad (\text{B11})$$

where we take $\bar{\rho}_{\text{MW}} = 0.4$ Gev/cm³ for the mean dark matter density, $\sigma = 100$ km/s, and the cloud mass and radius from (B5). It is expected that there are over 100 million neutron stars in the Milky Way but only 10^4 active radio pulsars [45]. This means that only 30 currently active pulsars have encountered at least once a scalar dark matter cloud. Moreover, for a given pulsar the encounter probability is only 0.3%. As we shall see below, this probability is even further reduced when we consider the capture rate.

2. Capture rate by dynamical friction

After the star enters the dark matter cloud, it will lose some energy by dynamical friction. We assume the

Chandrasekhar expression [46] for this drag force,

$$F_{\text{dyn}} = \frac{4\pi\rho\mathcal{G}^2 m_\star^2}{v^2} \Lambda, \quad (\text{B12})$$

where Λ is the Coulomb logarithm, which we will take constant. Within an order of magnitude, this expression applies to a wide variety of regimes, from collisionless systems when v is larger than the velocity dispersion of the cloud [46, 47] to fuzzy and self-interacting scalar dark matter when the velocity is larger than the local speed of sound [3, 12, 48]. The energy loss as the star moves inside the cloud is $\Delta E = \int F_{\text{dyn}} d\ell$, which we estimate as

$$\Delta E = \frac{4\pi\rho\mathcal{G}^2 m_\star^2}{v_{\text{esc}}^2} \Lambda R. \quad (\text{B13})$$

Here we used that the star enters the cloud with a velocity $v \simeq v_{\text{esc}}$ because $v_\infty \ll v_{\text{esc}}$, as we check below. To become bound to the cloud, the star must lose enough energy, $\Delta E > E_{\text{init}}$, where $E_{\text{init}} = m_\star v_\infty^2/2$ is its initial energy. This gives the condition

$$v_\infty < v_{\text{max}} \quad \text{with} \quad v_{\text{max}}^2 = v_{\text{esc}}^2 \frac{3\Lambda m_\star}{2M} \ll v_{\text{esc}}^2. \quad (\text{B14})$$

Thus, we find indeed $v_\infty \ll v_{\text{esc}}$ because the mass of the star is much smaller than the mass of the cloud, $m_\star \ll M$. For dark matter clouds such as (B5) and a neutron star of mass $m_\star = 2M_\odot$, we obtain for $\Lambda = 1$

$$m_\star = 2M_\odot : \quad v_{\text{max}} = 0.5 \text{ km/s}. \quad (\text{B15})$$

This small value of v_{max} means that dynamical friction is quite inefficient to dissipate the kinetic energy of the star in one crossing of the cloud. Then, the capture rate is $\Gamma_{\text{cap}} = \Gamma_{\text{enc}}(< v_{\text{max}})$, with the maximum velocity (B14).

From Eq.(B10), with $v_{\text{max}} \ll \sigma$, we obtain

$$\Gamma_{\text{cap}} = \frac{3\sqrt{2\pi}\Lambda\mathcal{G}^2 \bar{\rho}_{\text{MW}} m_\star}{\sigma^3}, \quad (\text{B16})$$

which happens to be independent of the mass and density of the dark matter clouds (in the regime of validity). Over the Hubble time $t_H = 1/H$, this gives the probability of capture for a given neutron star

$$P_{\text{cap}} = \Gamma_{\text{cap}} t_H \simeq 4 \times 10^{-8}, \quad (\text{B17})$$

where we take $\bar{\rho}_{\text{MW}} = 0.4 \text{ GeV/cm}^3$ for the mean dark matter density, $m_\star = 2M_\odot$, $\sigma = 100 \text{ km/s}$ and $\Lambda = 1$. Therefore, a few neutron stars may be captured in the Milky Way, but the probability that a given pulsar is embedded in a dark matter cloud is extremely low. The relatively inefficient dissipation by dynamical friction yields a much reduced capture probability as compared with the encounter probability (B11).

3. Random location

In the previous sections we have derived the encounter and capture probabilities of distant stars. If the dark matter clouds cover a sufficiently large fraction of the Milky Way volume, they will contain neutron stars that simply happen to be located within the clouds. Assuming random and uncorrelated distributions of the stars and of the clouds, the volume fraction occupied by the clumps is $V_{\text{occ}}/V_{\text{tot}} = \bar{\rho}_{\text{MW}}/\rho$. This gives a probability to be located within a dark matter cloud

$$P_{\text{loc}} = \frac{\bar{\rho}_{\text{MW}}}{\rho} \simeq 10^{-10}, \quad (\text{B18})$$

for the cloud inner density (57). This is even smaller than (B17), so that most stars that are located within dark matter clouds were captured by dynamical friction (or other more efficient processes).

-
- [1] L. Hui, *Ann. Rev. Astron. Astrophys.* **59**, 247 (2021), 2101.11735.
 - [2] W. Hu, R. Barkana, and A. Gruzinov, *Physical Review Letters* **85**, 1158 (2000), ISSN 00319007.
 - [3] L. Hui, J. P. Ostriker, S. Tremaine, and E. Witten, *Phys. Rev. D* **95**, 043541 (2017), 1610.08297.
 - [4] P.-H. Chavanis, *Phys. Rev. D* **84**, 043531 (2011), 1103.2050.
 - [5] P. Brax, J. A. R. Cembranos, and P. Valageas, *Phys. Rev. D* **100**, 023526 (2019), 1906.00730.
 - [6] R. G. García, P. Brax, and P. Valageas (2023), 2304.10221.
 - [7] P. Brax and P. Valageas (2025), 2501.02297.
 - [8] P. Brax and P. Valageas (2025), 2502.12100.
 - [9] E. W. Kolb and I. I. Tkachev, *Phys. Rev. Lett.* **71**, 3051 (1993), hep-ph/9303313.
 - [10] E. W. Kolb and I. I. Tkachev, *Phys. Rev. D* **49**, 5040 (1994), astro-ph/9311037.
 - [11] A. Boudon, P. Brax, and P. Valageas, *Phys. Rev. D* **106**, 043507 (2022), 2204.09401.
 - [12] A. Boudon, P. Brax, and P. Valageas (2023), 2307.15391.
 - [13] P. Brax, P. Valageas, C. Burrage, and J. A. R. Cembranos, *Phys. Rev. D* **110**, 083515 (2024), 2402.04819.
 - [14] D. Blas, S. Gasparotto, and R. Vicente, *Phys. Rev. D* **111**, 042008 (2025), 2410.07330.
 - [15] A. Khmelnsky and V. Rubakov, *JCAP* **02**, 019 (2014), 1309.5888.
 - [16] H. Y. Schive, T. Chiueh, and T. Broadhurst, *Nature Physics* **10**, 496 (2014), ISSN 17452481.
 - [17] H. Kim, *JCAP* **12**, 018 (2023), 2306.13348.
 - [18] H. Kim and A. Mitridate, *Phys. Rev. D* **109**, 055017 (2024), 2312.12225.

- [19] A. Eberhardt, Q. Liang, and E. G. M. Ferreira (2024), 2411.18051.
- [20] J. Ellis, M. Fairbairn, G. Franciolini, G. Hütsi, A. Iovino, M. Lewicki, M. Raidal, J. Urrutia, V. Vaskonen, and H. Veermäe, *Phys. Rev. D* **109**, 023522 (2024), 2308.08546.
- [21] Y. Gouttenoire (2025), 2503.03857.
- [22] N. K. Porayko et al. (EPTA), *Phys. Rev. D* **111**, 062005 (2025), 2412.02232.
- [23] J. Antoniadis et al. (EPTA, InPTA), *Astron. Astrophys.* **685**, A94 (2024), 2306.16227.
- [24] C. Unal, F. R. Urban, and E. D. Kovetz, *Phys. Lett. B* **855**, 138830 (2024), 2209.02741.
- [25] Y.-M. Wu and Q.-G. Huang, *Phys. Rev. D* **111**, 063032 (2025), 2411.02915.
- [26] K.-Y. Choi, E. J. Chun, and J. Kim, *Phys. Dark Univ.* **30**, 100606 (2020), 1909.10478.
- [27] A. Cheek, L. Visinelli, and H.-Y. Zhang (2025), 2503.08439.
- [28] G. Cusin, C. Pitrou, M. Pijnenburg, and A. Sesana (2025), 2502.17401.
- [29] E. Madelung, *Z. Phys.* **40**, 322 (1927).
- [30] N. K. Porayko et al., *Phys. Rev. D* **98**, 102002 (2018), 1810.03227.
- [31] A. Afzal et al. (NANOGrav), *Astrophys. J. Lett.* **951**, L11 (2023), [Erratum: *Astrophys. J. Lett.* 971, L27 (2024), Erratum: *Astrophys. J.* 971, L27 (2024)], 2306.16219.
- [32] R. w. Hellings and G. s. Downs, *Astrophys. J. Lett.* **265**, L39 (1983).
- [33] C. Smarra et al. (European Pulsar Timing Array), *Phys. Rev. Lett.* **131**, 171001 (2023), 2306.16228.
- [34] G. Agazie et al. (NANOGrav), *Astrophys. J. Lett.* **951**, L10 (2023), 2306.16218.
- [35] S. Kawamura et al., *PTEP* **2021**, 05A105 (2021), 2006.13545.
- [36] T. Kinugawa, H. Takeda, A. Tanikawa, and H. Yamaguchi, *Astrophys. J.* **938**, 52 (2022), 1910.01063.
- [37] A. Boudon, P. Brax, P. Valageas, and L. K. Wong (2023), 2305.18540.
- [38] Y. Shao and X.-D. Li, *Mon. Not. Roy. Astron. Soc.* **477**, L128 (2018), 1804.06014.
- [39] P. Brax, J. A. R. Cembranos, and P. Valageas, *Phys. Rev. D* **101**, 023521 (2020), 1909.02614.
- [40] N. Esser, *Phys. Rev. D* **112**, 043021 (2025), 2505.05564.
- [41] E. Poisson and C. M. Will, *Gravity: Newtonian, Post-Newtonian, Relativistic* (Cambridge University Press, 2014).
- [42] W. Dehnen, D. E. McLaughlin, and J. Sachania, *Monthly Notices of the Royal Astronomical Society* **369**, 1688 (2006), astro-ph/0603825.
- [43] T. King III, W. R. Brown, M. J. Geller, and S. J. Kenyon, *The Astrophysical Journal* **813**, 89 (2015), URL <https://doi.org/10.1088/0004-637X/813/2/89>.
- [44] B. Anguiano, S. R. Majewski, C. R. Hayes, C. A. Prieto, X. Cheng, C. M. Bidin, R. L. Beaton, T. C. Beers, and D. Minniti, *The Astronomical Journal* **160**, 43 (2020), ISSN 1538-3881, URL <http://dx.doi.org/10.3847/1538-3881/ab9813>.
- [45] M. Camenzind, *Compact objects in astrophysics : white dwarfs, neutron stars, and black holes* (Springer Berlin, Heidelberg, 2007).
- [46] S. Chandrasekhar, *Astrophys. J.* **97**, 255 (1943).
- [47] J. Binney and S. Tremaine, *Galactic Dynamics: Second Edition* (Princeton University Press, 2008), rev - revised, 2 ed.
- [48] L. Berezhiani, B. Elder, and J. Khoury, *JCAP* **10**, 074 (2019), 1905.09297.